



LAWRENCE  
LIVERMORE  
NATIONAL  
LABORATORY

# Picosecond resolution soft x-ray laser plasma interferometry

J. Filevich, J.J. Rocca, M.C. Marconi, R.F. Smith, J.  
Dunn, R. Keenan, J.R. Hunter, S.J. Moon, J. Nilsen, A.  
Ng, V.N. Shlyaptsev

December 2, 2003

Applied Optics

## **Disclaimer**

---

This document was prepared as an account of work sponsored by an agency of the United States Government. Neither the United States Government nor the University of California nor any of their employees, makes any warranty, express or implied, or assumes any legal liability or responsibility for the accuracy, completeness, or usefulness of any information, apparatus, product, or process disclosed, or represents that its use would not infringe privately owned rights. Reference herein to any specific commercial product, process, or service by trade name, trademark, manufacturer, or otherwise, does not necessarily constitute or imply its endorsement, recommendation, or favoring by the United States Government or the University of California. The views and opinions of authors expressed herein do not necessarily state or reflect those of the United States Government or the University of California, and shall not be used for advertising or product endorsement purposes.

# Picosecond resolution soft x-ray laser plasma interferometry

**J. Filevich, J.J. Rocca, M.C. Marconi<sup>1</sup>**

*NSF ERC for Extreme Ultraviolet Science and Technology and Department of  
Electrical and Computer Engineering, Colorado State University, Fort Collins,  
Colorado 80523*

**R.F. Smith, J. Dunn, R. Keenan, J.R. Hunter, S.J. Moon, J. Nilsen, A.**

**Ng**

*Lawrence Livermore National Laboratory, Livermore, California 94550*

**V.N. Shlyaptsev**

*Department of Applied Science, University of California Berkeley-Livermore,  
Livermore, California 94451*

---

<sup>1</sup>Permanent Address: Department of Physics, University of Buenos Aires, Buenos Aires, Argentina.

We describe a soft x-ray laser interferometry technique that allows two-dimensional diagnosis of plasma electron density with picosecond time resolution. It consists of the combination of a robust high throughput amplitude division interferometer and a 14.7 nm transient inversion soft x-ray laser that produces  $\sim 5$  ps pulses. Due to its picosecond resolution and short wavelength scalability, this technique has potential for extending the high inherent precision of soft x-ray laser interferometry to the study of very dense plasmas of significant fundamental and practical interest, such as those investigated for inertial confined fusion. Results of its use in the diagnostics of dense large scale laser-created plasmas are presented. © 2003 Optical Society of America

*OCIS codes:* 350.5400, 140.7240, 120.3180

## 1. Introduction

Since the advent of optical lasers, interferometry has been widely used to study different types of plasmas.<sup>1</sup> This powerful technique provides information in the form of two-dimensional maps of the electron density, often without the need of extensive modeling. However, when the plasma density approaches a fraction of a percent of the critical density, refraction and opacity effects can significantly limit these kind of diagnostics.<sup>2</sup> Refraction due to steep density gradients in the plasma can steer the probe beam completely out of the plasma, limiting the maximum plasma density and size that can be studied. In addition, at high plasma densities free-free absorption can attenuate the probe beam obscuring part of the interferogram. Nevertheless, both these adverse effects can be greatly reduced by significantly shortening the wavelength

of the probe beam. This constitutes the main motivation for pursuing soft x-ray laser interferometry. Soft x-ray lasers with wavelengths corresponding to critical densities in the range of  $5 \times 10^{23} - 5 \times 10^{24} \text{ cm}^{-3}$ , can potentially probe plasmas with densities up to two orders of magnitude larger than those accessible with optical lasers. In addition, x-ray lasers can provide the high brightness necessary to overcome the intense radiation emitted by hot dense plasmas.

The first demonstrations of soft x-ray plasma interferometry were performed with a 15.5 nm Ne-like Y laser pumped by the laboratory-size NOVA laser. In these initial proof-of-principle experiments Da Silva et al. demonstrated a Mach-Zehnder interferometer based on multilayer-coated thin film beam splitters.<sup>3,4</sup> With this interferometer, large (1-mm scale) plasmas were probed as close as 25  $\mu\text{m}$  from the initial target surface, where the electron density reached  $2 \times 10^{21} \text{ cm}^{-3}$ . More recently the versatility of soft x-ray laser interferometry was increased with the development of table-top lasers with peak spectral brightness that equals or exceeds that of their laboratory size predecessors.<sup>5,6</sup> Interferometry experiments performed at Colorado State University took advantage of a high repetition rate table-top capillary discharge pumped 46.9 nm laser<sup>5</sup> to obtain sequences of interferograms that map the evolution of laser created plasmas. Initial studies made use of a Lloyd's mirror interferometer,<sup>7,8</sup> and subsequent experiments used an amplitude division interferometer based on diffraction gratings.<sup>9</sup> However, the relatively long duration of the soft x-ray laser pulses used in these demonstrations (300 ps and 1.2 ns for the Ne-Like Y and Ne-like Ar lasers respectively) makes the interferograms susceptible to the blurring of the interference fringes which results from the rapid local variations of the electron density, during the

exposure time within a fast moving plasma. While these pulse widths are adequate for mapping the density of numerous slowly evolving dense plasmas, such as pulse-power plasmas and laser-created plasmas far from the target surface, it precludes their use in diagnosing plasmas where fast evolving steep density gradients lead to blurring of the fringes.

In this paper we describe a soft x-ray laser interferometry technique<sup>10</sup> that is capable of picosecond resolution plasma probing, which overcomes the limitations imposed by the rapid plasma motion. It consists of the combination of a robust high throughput amplitude division interferometer and a 14.7 nm laser that produces  $\sim 5$  ps pulses. The interferometer is a modification of the Diffraction Grating Interferometer (DGI) used in the capillary discharge soft x-ray laser interferometry experiments. It combines the advantages of increased resistance to damage by plasma debris with a high throughput of 6 percent per arm. The picosecond soft x-ray laser probe is the saturated output of the 14.7 nm Ni-Like Pd transient inversion scheme.<sup>6</sup> Both the DGI and the transient inversion laser are scalable to significantly shorter wavelengths (e.g. utilizing the 7.36 nm line of Ni-like Sm<sup>11</sup>). This, combined with the picosecond resolution of this technique have potential for extending the high inherent precision of soft x-ray laser interferometry to the study of very dense plasmas of significant fundamental and practical interest, such as those investigated for inertial confined fusion. The next section briefly reviews several designs of soft x-ray laser interferometers, and describes the DGI design and its alignment procedure. Section 3 presents results of dense plasma diagnostics utilizing this picosecond resolution soft x-ray laser interferometry technique.

## 2. Soft X-Ray Laser Interferometers

The main limitation in the construction of interferometers for the soft x-ray region of the spectrum has been the development of adequate beam splitters. Another limiting factor is the availability of mirrors with sufficiently high reflectivity to achieve a useful throughput. The beam splitters can be avoided by working with wave-front division interferometers instead. In these schemes, the probe beam is divided spatially to provide the reference and probe arms of the interferometer. The reflectivity requirements can be met, in some cases, by the use of grazing incidence reflections, and in others, with high reflectivity multilayer soft x-ray mirrors. However, the wave-front division interferometers have the drawback of a higher requirement on the spatial coherence of the laser source. This limitation can be overcome by placing the source far away from the interferometer as, according to the Huyghens-Fresnel principle,<sup>12</sup> the beam's transverse coherence increases with the distance from the source. In that case the coherence requirement translates into increased photon fluence.

The simplest interferometer that can be constructed is based on the Lloyd's mirror configuration.<sup>13</sup> This interferometer was implemented in combination with a soft x-ray laser by Rocca et al.,<sup>7</sup> and it was used in the diagnostic of a pinch plasma.<sup>8</sup> It consists of a reflection in a grazing incidence mirror that intercepts a portion of the beam from the soft x-ray laser source. The fringe pattern arises from the superposition of this portion of the beam with the one that propagates directly from the source. Due to the single grazing reflection this interferometer has high throughput. The fringe spacing is determined by the angle of incidence, and the distances from the point source to

the mirror and from the mirror to the image plane. The plasma to be probed is placed in one of the two portions of the beam, while the other portion is used as a reference. The maximum transverse plasma size that can be probed is determined by the mirror length and the angle of incidence on the mirror, and by the spatial and temporal coherence of the laser. The Fresnel Bi-mirror Interferometer<sup>13</sup> is almost as simple as the Lloyd's Mirror. It consists of two flat mirrors joined together at one side with a slight tilt between them. The light incident at a grazing angle on the mirrors is reflected, and due to this tilt, overlapped with itself generating interference fringes. This interferometer was used in combination with a 21.2 nm Ne-like Zn soft-x-ray laser by Albert et al.,<sup>14</sup> and was demonstrated in studying the effect of high electric fields on Nb surfaces.<sup>15</sup> Amplitude division interferometers do not have the limitation on the spatial coherence of the laser source, and can probe larger objects. The first amplitude division soft x-ray laser interferometry experiment was performed using a Ne-like Y 15.5 nm soft x-ray laser pumped by the laboratory size NOVA laser. Da Silva et al. demonstrated the technique for plasma diagnostics using an interferometer that utilized Mo-Si thin-film multilayer-coated beam splitters and mirrors mounted in a Mach-Zehnder configuration.<sup>16</sup> This interferometer was used to probe millimeter scale plasmas at distances as close as 25  $\mu\text{m}$  from the initial target surface where the measured electron density reached  $2 \times 10^{21} \text{cm}^{-3}$ .<sup>3</sup> It was also used to perform studies of the coherence length of the soft x-ray laser.<sup>4</sup> These experiments were the first to realize soft-x-ray interferometry of dense plasmas. However, the low repetition rate of the laboratory size x-ray lasers used and the fragile beam splitters that had to be replaced after every shot limited the amount of data that could be taken. Furthermore,

the 300 ps pulse duration of the probe laser limits the types of plasmas that can be studied due to the possible blurring of the interference fringes. Another amplitude division interferometer, a Michelson interferometer based on multilayer foil beam-splitters that provided transmission and reflectivity of 15 % and 14 % respectively, was recently constructed and used to measure the longitudinal coherence length of the Ni-Like Pd 14.7 nm soft-x-ray laser.<sup>17</sup> The use of these types of instruments is limited to the wavelength range in which low absorption thin film multilayer beam splitters can be manufactured.

The interferometer used to implement the picosecond resolution plasma diagnostics tool described in this paper uses reflective diffraction gratings as beam splitters.<sup>18,19</sup> The use of diffraction gratings allows the construction of amplitude division interferometers of increased robustness and high throughput that can be designed to operate over an extended range of soft x-ray wavelengths. The diffraction grating interferometer (DGI) was first demonstrated in combination with a 46.9 nm capillary discharge soft-x-ray laser, and it was used to unveil two-dimensional phenomena in line-focus and spot-focus laser created plasmas.<sup>19,20</sup> The DGI described in this paper is a modified version designed to operate at the 14.7 Ni-like Pd soft-x-ray laser wavelength with picosecond pulse duration. A description of this instrument, its alignment procedure, and its use for laser created plasma diagnostics are given in the next sections.

### 3. Diffraction Grating Interferometer

The DGI is set in a skewed Mach-Zehnder configuration as shown in Figure 1. The light incident on the first grating (G1) is diffracted with approximately equal intensity in the zero and first orders. These two beams that form the two arms of the interferometer are reflected at 2.6 degrees grazing incidence angle toward a second  $7.6 \times 8.5 \text{ cm}^2$  diffraction grating (G2) using two 35 cm long Au-coated mirrors (L1 and L2). Grating G2 recombines the two beams such that they exit the interferometer propagating with a small angular difference, selected to produce fringes of the spacing required by the particular experiment. By simulating the grating's performance,<sup>21</sup> a line spacing of 900 lines/mm and a blaze angle of 2 degrees were chosen. This grating diffracts the beam into a zero and a first order component of approximately the same intensity when operating at an incidence angle of 6 degrees. For the selected ruling and angle of incidence, the resulting angle between the zero and first diffracted orders is 5.2 degrees. This dispersion angle defines the geometry of the interferometer. Thus, with the two gratings separated by 90 cm center-to-center, the resulting distance between the two arms of the interferometer at the target position indicated in Fig. 1 is  $\sim 1$  cm. There, the phase object of interest, in our case a laser created plasma, is placed. The reflectivity of the gold-coated diffraction gratings is maximized by the small grazing incidence angle used, resulting in an efficiency of 25 % per order on each grating. The long mirror's (L1 and L2) reflectivity is  $\sim 90\%$ , giving a total throughput for the instrument of  $\sim 12\%$ .

Due to the wavelength-dependent dispersion of the gratings, the alignment of the

interferometer cannot, in principle, be performed with an auxiliary optical laser. To overcome this difficulty the diffraction gratings were designed to have two different, vertically separated, ruled sections on the same substrate. The section associated with alignment had a line spacing chosen to produce the same dispersion for a selected infrared (IR) laser diode as the dispersion of the soft x-ray laser on its ruled section. This IR laser diode for alignment is chosen to have a temporal coherence length similar or shorter than that of the soft x-ray laser ( $\sim 400$  microns  $1/e$  HW).<sup>17</sup> This ensures that the arm lengths are matched with sufficient precision to warrant the observation of fringes with the soft x-ray laser. The laser diode chosen<sup>22</sup> has a central wavelength of 827 nm and an estimated coherence length of  $\sim 300$   $\mu\text{m}$ . This wavelength determines the line density of the alignment ruling to be 16 lines/mm. Specifically, the gratings have a central region with 900 lines/mm for the soft x-ray laser radiation, and two other regions situated on top and below that have 16 lines/mm rulings to be used with the infrared laser diode. This 3-stripe ruling design permits the rotation of the second grating in order to reverse the blaze angle direction as is needed to recombine the two soft x-ray laser beams with equal intensities. The soft x-ray laser beam at the target position is imaged onto a  $1.33 \times 1.33$   $\text{cm}^2$  charged-coupled device (CCD) with  $1024 \times 1024$  pixels of  $13 \times 13$   $\mu\text{m}^2$  size.<sup>23</sup> The imaging optics consist of a 25 cm focal length Mo/Si multilayer spherical mirror (S1), set at 5 degrees off normal incidence, followed by an elongated Au-coated mirror (L3), positioned at a grazing angle of 9 degrees that relays the beam via a flat 45 degrees Mo/Si multilayer mirror to the CCD detector located approximately 5.5 meters away from the imaging mirror. This imaging set up has a total magnification of  $22 \times$  that was measured by imaging a

12.7  $\mu\text{m}$  spacing mesh placed at the target plane position (object plane of S1 mirror). This means a single CCD pixel is equivalent to 0.6  $\mu\text{m}$  at the object plane and the overall system spatial resolution is determined to be  $\sim 2 \mu\text{m}$ .

To align the DGI, a 632.8 nm He-Ne laser beam is first pointed along the input path of the soft x-ray beam into the first grating. This visible beam is then steered with G1, L1 and G2 along the zero order arm into the detector. The first order alignment is then performed using the 16 lines/mm secondary ruling and the 827 nm IR laser diode. The IR laser diode is steered along the zero order path using two Al-coated mirrors, to assure that the incidence angle on the first grating is correct. The first diffracted order beam is subsequently adjusted using L2, to follow the first order arm of the interferometer. Final corrections of L2 and G2 are made until the fringes are clearly observed at the output of the DGI. At this stage of the alignment the orientation (vertical or horizontal) of the fringes can be chosen. Also, for its use in plasma diagnosis, it is usually advantageous to assure that the angle between the beams is such that a plasma set on the zero order beam will produce fringe shifts away from the target. This often facilitates the interpretation of the fringe shifts for the determination of the electron density profile. Since the height of the IR beam is different from that of the soft x-ray laser beam, the alignment through the imaging optics onto the detector is done with the visible He-Ne laser using the zero order arm.

Due to the difficulty in obtaining a good blaze profile on very small groove densities, the IR ruling is effectively not blazed. As a result, most of the IR energy is diffracted onto the zero order, creating a large intensity difference between the two arms of the DGI, when aligning. This prevents the fringes from the IR alignment laser

to be observed at the output of the DGI. However the first diffracted order off the second grating can be used instead for this purpose. In this case the intensity of both orders is similar, because each undergoes a reflection (zero order) and a first order diffraction. As the optimum alignment can differ slightly from that obtained with the IR beam the final adjustments are conducted under vacuum with the soft x-ray laser beam, utilizing motorized actuators to control the position of the relevant optics. We discovered that some of the movements are more critical than others. For example, it was found there is no need to motorize G1. In contrast, the translations of L1 and L2 are important, and it is useful to have these axes encoded since they provide control of the overlap between the beams of the two arms. The horizontal and vertical tilt of L2 and G2 are used very frequently to orient the fringes and to select the desired fringe spacing. L1 vertical and horizontal tilts are used, but not as often as those on L2. The translation of G2 is also used but less frequently. It is important to have the imaging mirror translation motorized to be able to adjust the focus and produce a sharp image of the target on the detector. The horizontal and vertical tilt of both this mirror and the relay mirror (L3) are used to steer the beam into the CCD camera, but it is possible to operate with only adjusting the relay mirror tilt, if it is found that only small corrections are required.

The combination of a CCD camera placed inside the DGI chamber with two flip-in mirrors allowed the monitoring of the soft x-ray laser beam at the input and at the output of the interferometer. In this way, the pointing of the soft x-ray at the input of the DGI could be compared with that of the He-Ne laser used to align it. The relatively low magnification ( $8.5 \times$ ) of the optics used to image the output of the

interferometer allowed the monitoring of the beams corresponding to the two arms of the interferometer. The magnification was such that nearly the entire intensity footprint of the x-ray laser beam was visible for both arms simultaneously. This is essential for the final alignment of the DGI because it provides information on the overlap, the intensity distribution and quality of the fringes.

#### 4. Picosecond Resolution Plasma Probing

To demonstrate soft x-ray laser interferometry with picosecond resolution the DGI was combined with a transient 14.7 nm Ni-like Pd soft x-ray laser.<sup>6</sup> The soft x-ray laser was pumped by two beams from a chirped pulse amplification laser, the Compact Multipulse Terawatt (COMET) system at LLNL that operates at 1054 nm. An x-ray laser output of a few 10's of  $\mu\text{J}$  was achieved by optically pumping a polished Pd target with a sequence of a 600 ps long pulse ( $2 \text{ J}$ ,  $2 \times 10^{11} \text{ Wcm}^{-2}$ ) and a 5 J energy 6.7 ps or 13 ps (FWHM) short pulse at an incident intensity of  $6 \times 10^{13} \text{ Wcm}^{-2}$  and  $3 \times 10^{13} \text{ Wcm}^{-2}$ , respectively. Traveling wave line focus excitation was achieved using a reflection echelon that consists of seven flat mirror segments placed before the focusing optics. Each mirror segment was offset by 0.12 cm to introduce the traveling wave toward the output of the laser with a delay of 7.7 ps per step. This results in a phase velocity of  $c$  along the line focus length and ensures that peak gain conditions are experienced by the propagating x-ray laser photons. The horizontal angular divergence of the soft x-ray laser was measured to be 2.8 mrad. The near field and far field beam characteristics were studied and the laser parameters were optimized to obtain beam properties suitable to perform interferometry. It was

decided to relay image the x-ray laser exit pattern from the end of the Pd target to the target plane inside the interferometer. This made the x-ray laser beam alignment insensitive to shot-to-shot variation in deflection angle exiting the Pd plasma. Beam pointing stability was better than  $25 \mu\text{rad}$ . This was achieved by using a spherical 0 degree Mo/Si multilayer coated mirror with 11.75 cm focal length at the end of the Pd plasma and an encoded flat 45 degree Mo/Si multilayer coated mirror to point the x-ray beam onto the first interferometer grating G1. The temporal properties of the x-ray laser have been recently measured with a fast x-ray streak camera under the same laser pumping conditions as the interferometry experiments.<sup>24</sup> Figure 2 shows a sample streak lineout with an x-ray pulse duration of 4.7 ps (FWHM) with an approximately Gaussian shape for a 6.7 ps short pump pulse. For saturated x-ray laser output the x-ray duration is typically in the range of 4.5 - 5.2 ps. With the longer 13 ps pumping pulse, the measured x-ray duration is slightly longer at 5.9 ps.<sup>24</sup> This short pulse duration permits the acquisition of “snap-shots” of the rapidly evolving plasma, overcoming the blurring of interference fringes that occur when the electron density profile changes significantly during the duration of the probe pulse. The combination of the robust grating interferometer with the relatively high repetition rate picosecond soft x-ray laser (1 shot every 4 minutes) permitted the acquisition of sequences of interferograms that map the evolution of the electron density distribution in high density laser created plasmas.

Figure 3(a) shows a typical “reference” interferogram obtained without the plasma present. Figure 3(b) shows the fringe intensity as a function of the position away from the target, taken along the dashed line between the points A-A’. Some variation in

intensity is visible due to mode structure within the x-ray laser beam. However, the visibility,  $V = \frac{I_{max} - I_{min}}{I_{max} + I_{min}}$  calculated from this plot, and shown in Fig. 3(c), is excellent with regions with over 0.8 visibility observed. Taking into account that for plasma probing experiments good intensity is also needed to overcome absorption and intense plasma self-emission, this interferogram shows that the region suitable for plasma diagnostics is at least  $300 \times 700 \mu m^2$ . Plasma probing was achieved by generating a laser-produced plasma at a position half way between the elongated mirror (L1) and the second grating (G2) along the trajectory of the zeroth order arm of the interferometer (location marked as “target” in Fig 1). The targets were mounted on a motorized manipulator that allowed motion along all three axes. The rotation around the vertical axis was also controlled using a stepper motor to facilitate the alignment of the target surface parallel to the x-ray probe beam. This angular alignment was better than 0.25 degree and reduces the shadowing of the fringes by a 1 mm long target to  $2 \mu m$ . The rotations around the axis parallel and perpendicular to the target surface were also motorized to allow alignment with respect to the heating beam. The plasma was generated with a  $1 \omega$  (1054 nm) wavelength, 40 mm diameter beam from the COMET laser, which provides up to 3 J of energy in a 600 ps (FWHM) pulses. A  $\sim 20 \mu m$  wide 3.1 mm long line focus was generated on the target surface using the combination of a 200 cm focal length cylindrical lens and a 30 cm focal length off-axis paraboloid. The 1 mm long targets were overfilled to obtain a uniform heating of the plasma. The line focus size and homogeneity were measured by imaging the plasma heating beam at the target plane with a through imaging system consisting of an achromatic lens and a series of relay mirrors that redirected the beam to a

CCD camera. To limit the amount of plasma self emission collected by the imaging CCD a 1 mm pinhole (not shown in Figure 1) was placed between G2 and IM. The pinhole reduces the collection angle of the imaging system, thus reducing the amount of plasma x-ray self-emission recorded. To further block the stray optical light from the plasma-forming laser and from the plasma, a 2000 Å Zr + 1000 Å polyimide ( $C_{22}H_{10}N_2O_5$ ) filter was placed in front of the CCD camera.

Figure 4 (a-d) shows a sequence of interferograms that describe the evolution of a 1 mm long plasma generated by heating a flat titanium target with the line focus beam described above. The interferograms correspond to time delays of -0.5, 0, 0.5 and 1.5 ns measured respect to the peak of the 600 ps heating laser pulse. Figure 4(a) corresponds to a time shortly after the initiation of the plasma. In the subsequent three frames of the evolution plasma expansion is observed to have a very significant component along the target surface direction, a characteristic that emphasizes its two-dimensional nature. Figure 5 shows the calculated density maps obtained from the interferograms in Fig. 4. Figure 5c, which corresponds to 0.5 ns after the peak of the 600 ps heating laser pulse shows a maximum density of  $5.5 \times 10^{20} \text{ cm}^{-3}$  measured at a distance of 2  $\mu\text{m}$  from the original target surface. A second type of target investigated was a groove in aluminum 100  $\mu\text{m}$  wide and 200  $\mu\text{m}$  deep as shown in the reference interferogram in Fig. 6. (a). Beam 3 of COMET laser was used to heat the bottom of the groove with 3 J in a tight  $\sim 12 \mu\text{m}$  wide, 3.1 mm long line focus. The shot shown in Fig 6 (b) illustrates an interferogram obtained at 1.25 ns after the peak of 600 picoseconds heating laser pulse. The evolution of the plasma inside the groove has very different characteristics from that corresponding to a flat target. The very

large and rapid lateral expansion of the plasma is constrained by the groove walls, forcing the plasma toward the center of the groove. The local maximum on axis can be interpreted as the collision of plasma arising from the walls. The electron density map, Fig 6. (c), shows this axis enhanced density. This example illustrates that picosecond soft x-ray laser probes create the opportunities to study collisions and stagnation in large scale plasmas. A more complete study of the evolution of these plasmas will be published separately.

Two dimensional maps of the electron density were constructed by measuring the number of fringe shifts for different positions on the interferograms. For the axially uniform plasma of length  $L$  discussed herein, the fringe shifts  $N_{fringe}$  observed in the interferograms are associated with a plasma electron density by<sup>25</sup>

$$N_{fringe} = \frac{\delta\phi}{2\pi} = \frac{1}{\lambda} \int_0^L (1 - n_{ref}) dl \approx \frac{n_e}{2n_{crit}} \cdot \frac{L}{\lambda}$$

Where  $\delta\phi$  is the phase shift, and the index of refraction  $n_{ref} = (1 - n_e/n_{crit})^{\frac{1}{2}}$  is a function of the electron density,  $n_e$ , and the critical density  $n_{crit} = 1.1 \times 10^{21} \lambda^{-2}$  (in  $cm^{-3}$ , for the probe laser wavelength  $\lambda$  in  $\mu m$ ). It is useful to express the electron density as a function of the observed fringe shifts:  $n_e = 2.2 \times 10^{21} N_{fringe} \cdot \frac{1}{\lambda \cdot L}$  where  $L$  and  $\lambda$  are expressed in micrometers. For the 14.7 nm wavelength of the probe laser and 1 mm length of the plasmas discussed herein, one fringe shift corresponds to a density of  $1.5 \times 10^{20} cm^{-3}$ . In principle the minimum density increment  $\Delta n_e$  that can be measured depends on the minimum detectable fringe shift. If the fringes were perfectly straight the  $\sim 30$  pixels between lines in the interferograms shown here, would correspond to an error in the determination of the plasma electron density

of  $\Delta n_e \sim 2.5 \times 10^{18} \text{cm}^{-3}$ . However, in our case, undulations in the fringes due to the mode structure of the laser that varies from shot to shot limits the accuracy with which the reference fringes can be determined, increasing the uncertainty. An estimated uncertainty of 10 - 20 % in the determination of the reference fringes for the case of the 1mm long plasma results in an error of  $1.5 - 3 \times 10^{19} \text{cm}^{-3}$  in the electron density. An additional phenomenon that can introduce errors in plasma probing experiments is the extent to which the probe beam is deflected by refraction in the plasma medium.<sup>26</sup> The large density gradients encountered in laser-created plasmas close to the target can produce significant steering of the probe beam away from the highest density regions. Knowledge of the extent and effect of refraction is therefore an important consideration for accurate analysis of the data. A grid reflectometry study was performed with the DGI<sup>27</sup> to estimate these refraction effects in 1mm long plasmas such as those investigated herein. That study showed that the present data can be analyzed without the need of a correction due to refraction. This is in contrast with the use of an ultraviolet laser probe (e.g. the third harmonic of YAG, 267 nm), whose beam would have been strongly refracted away from the region close to the target shortly after entering the 1 mm long plasma, making the probing of that region unfeasible.

## 5. Conclusions

Interferometry of dense plasmas at a wavelength of 14.7 nm has been demonstrated with picosecond resolution. The combined picosecond resolution and ultrashort wavelength of this technique has potential for extending plasma interferometry significantly

beyond the limits of current methods. The instrumentation developed for this purpose combines an amplitude division interferometer that uses diffraction gratings as beam splitters with the 14.7 nm output of the Ni-like Pd transient soft x-ray laser. The grating interferometer combines the advantages of excellent fringe visibility over a large area with high throughput and good resistance to damage by the plasma. Several hundred plasma shots were performed with laser heating energies of up to 150 J without any observable damage or deterioration on the image quality. Densities up to  $4.5 \times 10^{20} \text{cm}^{-3}$  were measured at distances as short as  $2 \mu\text{m}$  from the target in different types of millimeter size line focus laser-created plasmas. The instrumentation and methodology developed is scalable to significantly shorter wavelengths, and constitutes a promising scheme for extending interferometry to the study of very dense plasmas such as those investigated for inertial confined fusion.

## **Acknowledgments**

The authors would like to thank Albert Osterheld of LLNL for continued support of this work. In addition, the authors are grateful to Ronnie Shepherd and Rex Booth of LLNL for their help in the measurement of the x-ray laser pulse duration. This work was supported by U.S. Department of Energy grant No. DE-FG03-02NA00062. Part of this work was performed under the auspices of the U.S. Dept. of Energy by the University of California, Lawrence Livermore National Laboratory through the Institute of Laser Science and Application, under contract No. W-7405-Eng-48. This work made use of Engineering Research Centers Facilities supported by the National Science Foundation under award number EEC-0310717. The CSU researchers also

gratefully acknowledge the support of the W.M. Keck Foundation.

## References

1. T.P. Hughes. *Plasma and Laser Light*. John Wiley and Sons, New York, 1975.
2. R.A. Alpher and D.R. White. *Optical Interferometry*, pages 431– 476. *Plasma Diagnostic Techniques*. Ed. R.H. Huddlestone and S.L. Leonard. Academic Press, New York, 1965.
3. L. B. Da Silva, T. W. Barbee Jr., R. Cauble, P. Celliers, D. Ciarlo, S. Libby, R. A. London, D. Matthews, S. Mrowka, J. C. Moreno, D. Ress, J.E. Trebes, A. S. Wan, and F. Weber. Electron density measurements of high density plasmas using soft x-ray laser interferometry. *Physical Review Letters*, 74(20):3991, 1995.
4. P Celliers, F Weber, L.B. Da Silva, T. W. Barbee, R. Cauble, Jr., A. S. Wan, and J. C. Moreno. Fringe formation and coherence of a soft-x-ray laser beam illuminating a Mach-Zehnder interferometer. *Optics Letters*, 20(18):1907, 1995.
5. B. R. Benware, C. D. Macchietto, C. H. Moreno, and J. J. Rocca. Demonstration of a high average power tabletop soft x-ray laser. *Physical Review Letters*, 81(26):5804–5807, 1998.
6. J. Dunn, Y. Li, A. L. Osterheld, J. Nilsen, J. R. Hunter, and V. N. Shlyaptsev. Gain saturation regime for laser-driven tabletop, transient Ni-like ion x-ray lasers. *Physical Review Letters*, 84(21):4834–4837, 2000.
7. J. J. Rocca, C. H. Moreno, M. C. Marconi, and K. Kanizay. Soft-x-ray laser interferometry of a plasma with a tabletop laser and a Lloyd’s mirror. *Optics Letters*, 24(6):420–422, 1999.

8. C. H. Moreno, M. C. Marconi, K. Kanizay, J. J. Rocca, Y. A. Uspenskii, A. V. Vinogradov, and Y. A. Pershin. Soft-x-ray laser interferometry of a pinch discharge using a tabletop laser. *Physical Review E*, 60(1):911–917, 1999.
9. J. Filevich, K. Kanizay, M. C. Marconi, J. L. A. Chilla, and J. J. Rocca. Dense plasma diagnostics with an amplitude-division soft-x-ray laser interferometer based on diffraction gratings. *Optics Letters*, 25(5):356–358, 2000.
10. R. F. Smith, J. Dunn, J. Nilsen, V. N. Shlyaptsev, S. Moon, J. Filevich, J. J. Rocca, M. C. Marconi, J. R. Hunter, and T. W. Barbee. Picosecond x-ray laser interferometry of dense plasmas. *Physical Review Letters*, 89(6):065004, 2002.
11. J.Y. Lin, G. J. Tallents, J. Zhang, A.G. MacPhee, C.L.S. Lewis, D. Neely, J. Nilsen, R.M.N. Pert, G.J. and O'Rourke, R. Smith, and E. Wolfrum. Gain saturation of Ni-like x-ray lasers. *Optical communications*, 158:55, 1998.
12. M. Born and E. Wolf. *Elements of the theory of diffraction*, pages 412–516. in Principles of Optics. Cambridge University Press, 7 edition, 1999.
13. M. Born and E. Wolf. *Elements of the theory of interference and interferometers*, pages 286–411. in Principles of Optics. Cambridge University Press, 7 edition, 1999.
14. F. Albert, D. Joyeux, P. Jaegle, A. Carillon, J.P. Chauvineau, G. Jamelot, A. Klisnick, J.C. Lagron, D. Phalippou, D. Ros, S. Sebban, and P. Zeitoun. Interferograms obtained with an x-ray laser by means of a wavefront division interferometer. *Optics Communications*, 142:184–188, 1997.
15. Ph. Zeitoun, F. Albert, P. Jaegl, D. Joyeux, M. boussoukaya, A. Carillon, S. Hu-

- bert, G. Jamelot, A. Klisnick, D. Phalippou, J.C. Lagron, D. Ros, S Sebban, and A. Zeitoun-Fakiris. Investigation of strong electric-field induced surface phenomena by xuv laser interferometry. *Nuclear Instruments and Methods in Physics Research A*, 416:189–191, 1998.
16. L. B. Da Silva, T. W. Jr. Barbee, R. Cauble, P. Celliers, J. C. Moreno, J. E. Trebes, Wan A. S., and F. Weber. Extreme-ultraviolet interferometry at 15.5 nm using multilayer optics. *Applied Optics*, 34(28):6389, 1995.
  17. R. F. Smith, J. Dunn, J. R. Hunter, J. Nilsen, S. Hubert, S. Jacquemot, C. Remond, R. Marmoret, M. Fajardo, P. Zeitoun, and L. Vanbostal. Longitudinal coherence measurement of a transient collisional x-ray laser. *Optics Letters*, 28(22):2261–2263, 2003.
  18. J. L. A. Chilla, J. J. Rocca, O. E. Martinez, and M.C . Marconi. Soft x-ray interferometer for single-shot laser linewidth measurements. *Optics Letters*, 21(13):955–957, 1996.
  19. J. Filevich, J. J. Rocca, E. Jankowska, E. C. Hammarsten, K. Kanizay, M. C. Marconi, S. J. Moon, and V. N. Shlyaptsev. Two-dimensional effects in laser-created plasmas measured with soft-x-ray laser interferometry. *Physical Review E*, 67(5):056409, 2003.
  20. J. J. Rocca, E. C. Hammarsten, E. Jankowska, J. Filevich, M. C. Marconi, S. Moon, and V. N. Shlyaptsev. Application of extremely compact capillary discharge soft x-ray lasers to dense plasma diagnostics. *Physics of Plasmas*, 10(5):2031–2038, 2003.

21. M. Seminario, J. J. Rocca, R. A. Depine, B. Bach, and B. Bach. Characterization of diffraction gratings by use of a tabletop soft-x-ray laser. *Applied Optics*, 40(30):5539–5544, 2001.
22. Laser diode SDL-5401-GL by SDL (<http://www.jdsu.com>).
23. Princeton Instruments PI-SX:1k. Roper Scientific, Inc. 3660 Quakerbridge Road. Trenton, NJ 08619.
24. J. Dunn, R.F. Smith, R. Shepherd, R. Booth, J. Nilsen, J.R. Hunter, and V.N. Shlyaptsev. Temporal characterization of a picosecond laser-pumped x-ray laser (for applications). In E.E. Fill, editor, *SPIE Int. Soc. Opt. Eng. Proc*, volume 5197, 2003. (in Press).
25. D. Attwood. *Soft X-Rays and Extreme Ultraviolet Radiation*, page 239. Physics of hot dense plasmas. Cambridge University Press, Cambridge, 2000.
26. R.S. Craxton, F.S. Turner, R. Hoefen, C. Darrow, E.F. Gabl, and G. E. Busch. Characterization of laser-produced plasma density profiles using grid image refractometry. *Physics of Fluids B*, 5(12), 1993.
27. R. F. Smith, J. Dunn, J. Nilsen, J. R. Hunter, V. N. Shlyaptsev, J. J. Rocca, J. Filevich, and M. C. Marconi. Refraction effects on x-ray and ultraviolet interferometric probing of laser-produced plasmas. *Journal of the Optical Society of America B: Optical Physics*, 20(1):254–259, 2003.

## List of figure captions

- Fig. 1. Experimental setup, depicting the Diffraction Grating Interferometer. The soft x-ray laser enters and exits the interferometer through the lower right side.
- Fig. 2. Temporal profile of the Ni-like Pd 14.7 nm x-ray laser probe emitted from a 1 cm target and pumped by a 6.7 ps short pulse. Pulse shape is approximately Gaussian with 4.7 ps (FWHM).
- Fig. 3. Interferogram obtained without the plasma present (a). Intensity plot versus the distance away from the target surface, between the points A-A' (b). Plot of the visibility of the fringes versus the distance away from the target surface (c).
- Fig. 4. Interferograms depicting the evolution of a titanium plasma heated with a 600 ps - 1.1 J - 20  $\mu\text{m}$  wide by 3.1 mm long line focus. The times shown are measured from the peak of the heating pulse. The targets are 1mm long.
- Fig. 5. Electron density maps obtained from the interferograms shown in Figure 4. The contour density lines represent a one decade step.
- Fig. 6. Reference interferogram showing a  $100 \times 200 \mu\text{m}$  Al groove target (a). Interferogram taken at 1.25 ns from the peak of the 600 ps - 3 J - line focus plasma heating beam into the groove target (b). Electron density map obtained from the interferogram in part (b) showing a maximum density of  $\sim 9 \times 10^{20} \text{cm}^{-3}$  measured near the walls.

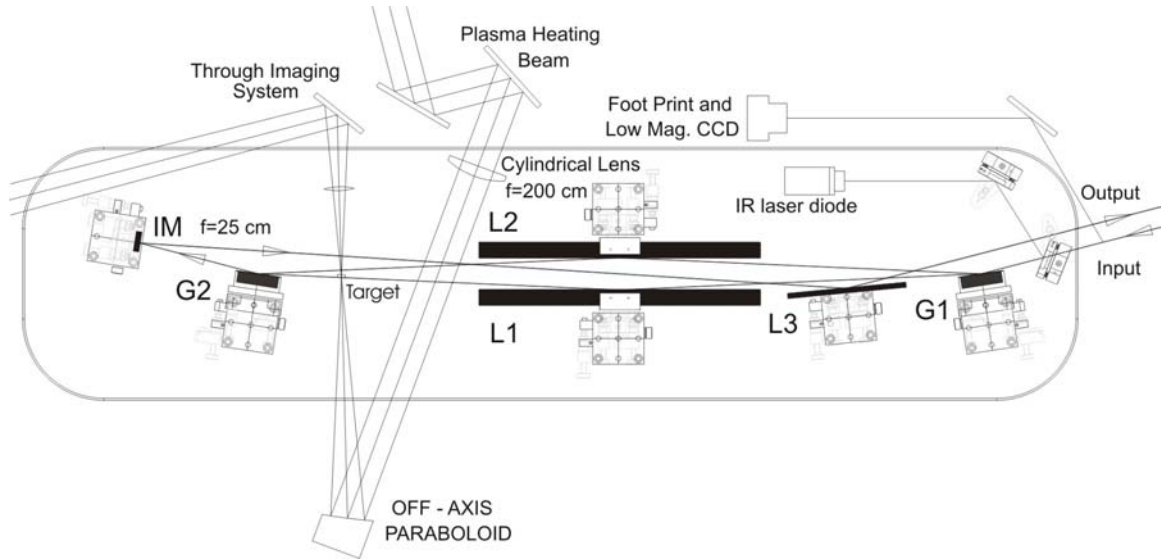


Figure 1

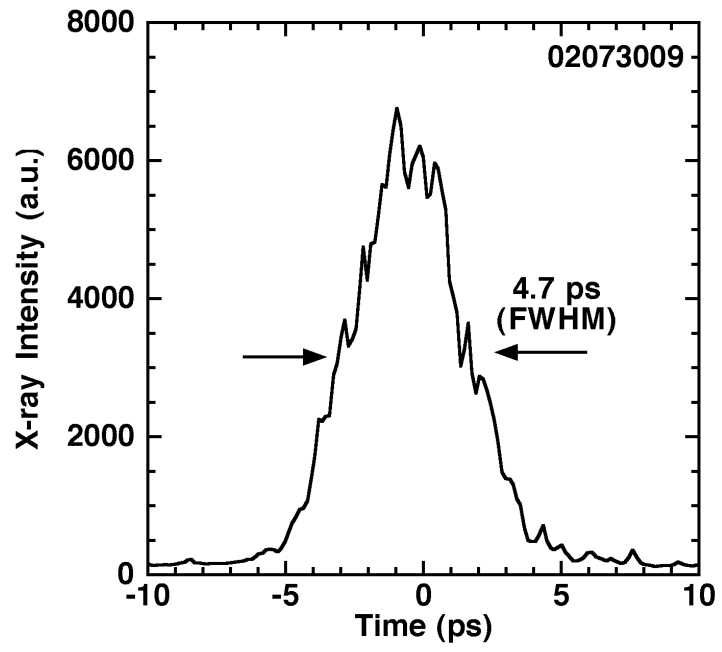


Figure 2.

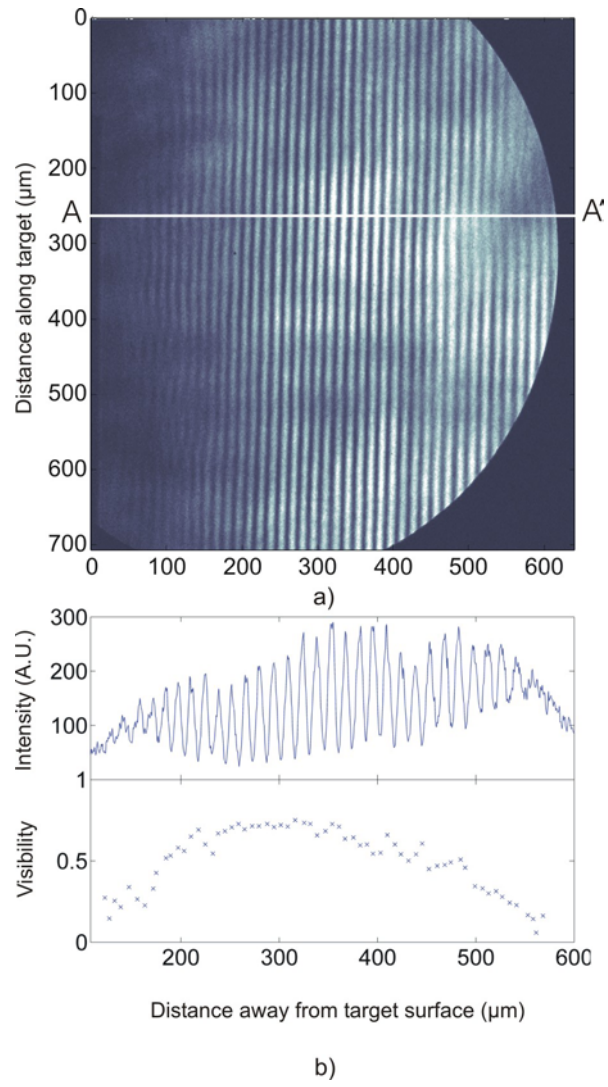


Figure 3.

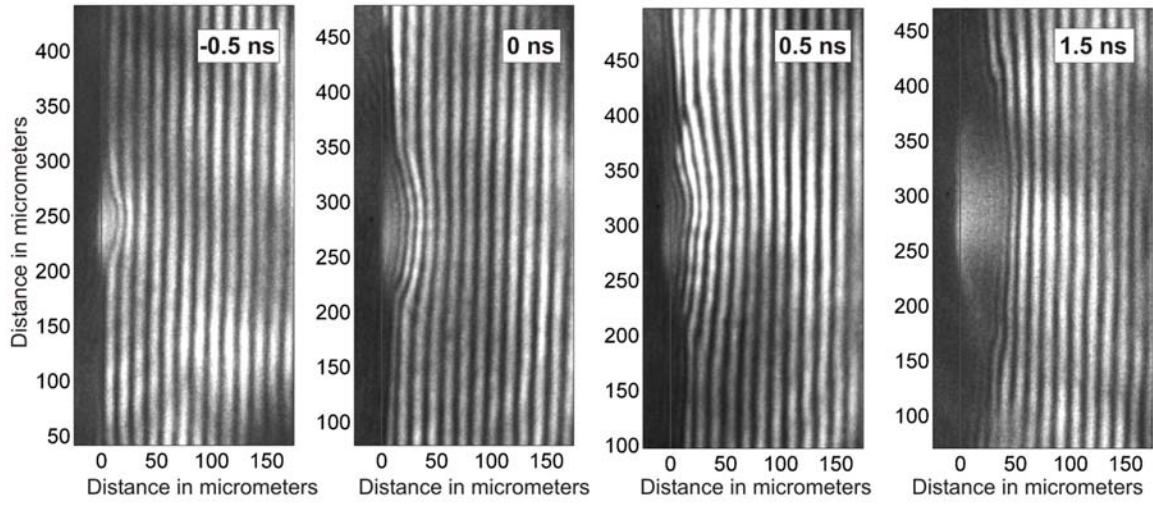


Figure 4.

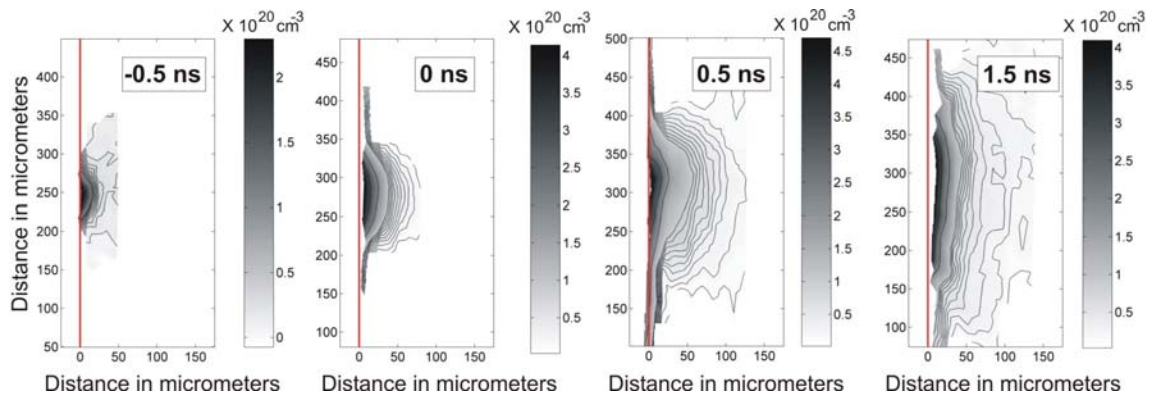


Figure 5.

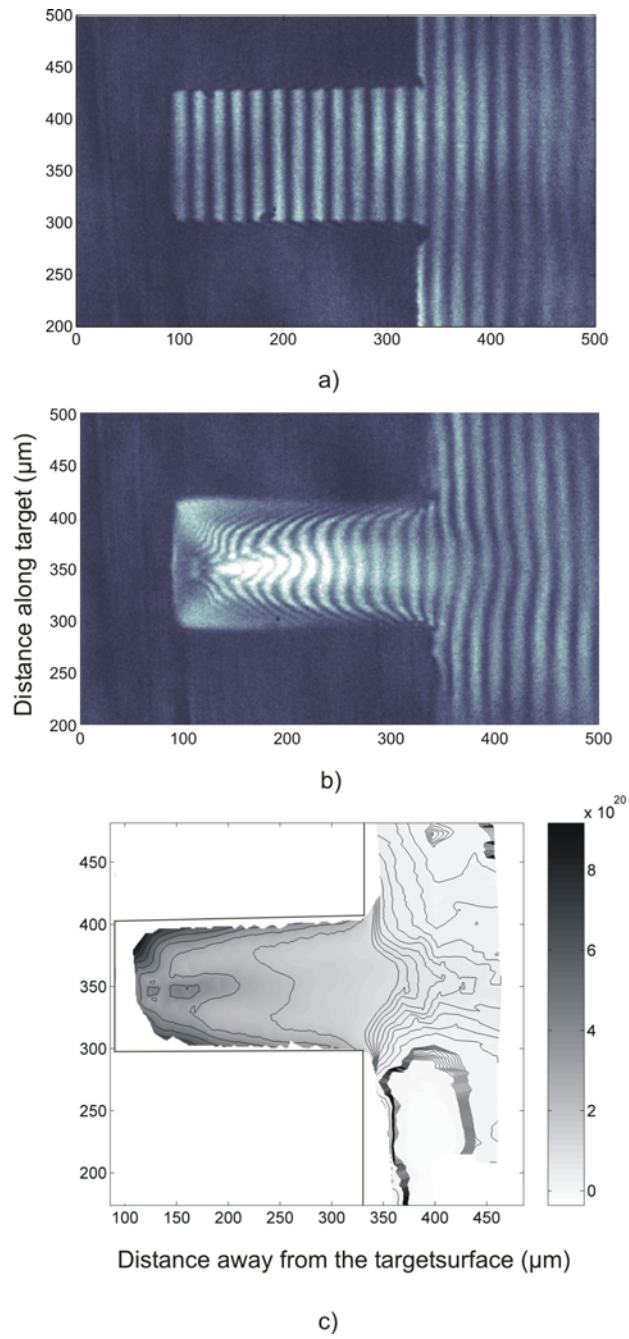


Figure 6.

University of California  
Lawrence Livermore National Laboratory  
Technical Information Department  
Livermore, CA 94551

